

Rotational Speed Control of Floating Wind Turbines

CA9

Martin Højlund Therkildsen

Technical Faculty of IT and Design
Department of Control and Automation

Frederik Bajers Vej 7C

9220 Aalborg East

Email: mtherk21@student.aau.dk

Supervisors

Torben Knudsen

Contacts at Vestas

Sune Baun Christensen

Jesper Sandberg Thomsen



Abstract

This project documents the multiple-inputs-multiple-outputs (MIMO) controller design of a reefer trailer refrigeration system.. and so on!

CONTENTS

1	Introduction	4
1.1	Problem definition	4
2	Theoretical Background	5
2.1	Aerodynamics and airfoil theory	5
3	System Description	7
4	Modelling	8
4.1	Aerodynamics	8
5	Controller Design	9
6	Conclusion	10
7	Future Work	11
	References	12
8	Appendix	13
8.1	Link to GitHub Repository	13
8.2	Explanation of relevant terms for thermodynamics	13
8.2.1	Enthalpy	13
8.2.2	Internal energy	13
8.3	List of table lookup symbols	13
8.4	Linearity of cargo heat transfer coefficient	13
9	Documentation and tests	14
9.1	Test Journal: Evaporator component model	14
9.1.1	Objective	14
9.1.2	Background	14
9.1.3	Test subject	14
9.1.4	Equipment used	14
9.1.5	Test setup	14
9.1.6	Test procedure	14
9.1.7	Results and Comments	14
9.1.8	Sources of error and insecurities	14

1 INTRODUCTION

In 2015 the United Nations set up the 17 Sustainable Development Goals. These outline global political actions that must be taken to achieve a better and more sustainable future for all. Each Goal describes a political, economical, social.. xxx

The global average temperature of the earth is rising. Mainly attributed to the greenhouse effect caused primarily by carbon dioxide (CO₂) emissions. The consequences of these temperature changes are aplenty and the more obvious signs of change are already starting to show. Record high temperatures, droughts, storms, floods and other extreme weather conditions and events are becoming more and more frequent. The main contributor to the release of CO₂ into the atmosphere is in the form of energy consumption. Energy use comes in many forms such as electricity generation, transportation, residential heating and industry. The energy demand on a global scale is still steadily increasing. Due to COVID-19 an unprecedented drop in energy use and CO₂ emissions were observed in 2020. But primary energy demand increased again in 2021 by 5.8 % which was 1.3 % higher than in 2019 [1]. Fossil fuel still makes up 82 % of the primary energy use in 2021 [1]. A transition from fossil energies to renewable energy sources is one of the most efficient remedies to lower CO₂ emissions. Solar and wind energy are widely accepted as some of the best green energy alternatives. Wind and solar reached a 10.2% share of power generation in 2021 [1]. As of 2021 236 GW of wind power capacity is installed in Europe with 12% being offshore. 17 GW was installed in 2021 alone with a 19 % share being offshore wind[2].

Despite offshore wind turbines (WTs) being more expensive to install than the onshore counterpart the trend towards offshore wind is increasing. There are sensible reasons for this. The offshore wind is on average 20% faster than onshore. Turbulence is also less due to the lack of obstacles at sea which could potentially extend the expected WT lifetime from 25 years to 30 years [3]. Furthermore wind farms at sea do not have the same clearance issues with regards to minimum distance from urban areas and houses. As a result visual and noise annoyances are also decreased. Issues with regards to offshore WTs is the shallow water depth requirement of most types of foundations. Above 50 meters water depth fixed-bottom offshore WTs start to become economically infeasible [4]. Shallow water depth sites will also eventually exhaust and it will become a necessity to install WTs at deeper waters. This is where the floating offshore wind turbine (FOWT) comes into play.

The FOWT is characterized by having a floating foundation in contrast to the classical fixed-bottom foundation which is connected directly to the sea floor.

1.1 Problem definition

2 THEORETICAL BACKGROUND

The purpose of this chapter is to go through the basic wind turbine (WT) theory.

2.1 Aerodynamics and airfoil theory

The sun delivers energy to the earth by heating up the surface and subsequently the air of the earth. Winds occur as a result of the pressure differences that occur due to the expansion and contraction of the air.

WTs work because they are able to convert the wind's energy into a torque in the generator which then generates electrical energy. When the wind blows over the blades of a WT it delivers some of its energy to the blade, yielding both a thrust force and torque to the blade.

In the simplest 1D momentum theory case the delivery of energy just results in a lowering of the wind speed following the rotor area. Due to mass retention an expansion would subsequently occur as seen in [Figure 1](#). The energy in the wind can

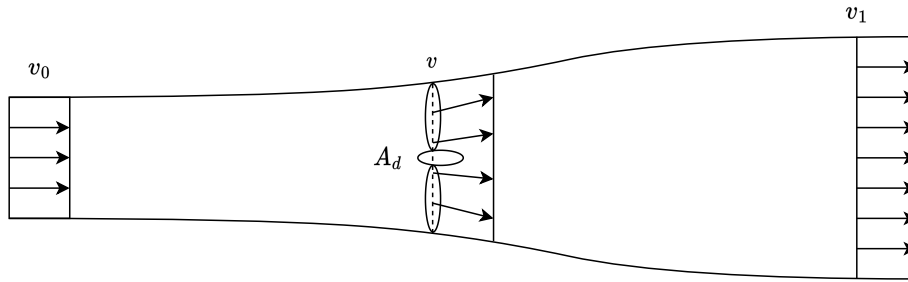


Figure 1: Illustration of how the wind in a control volume (CV) changes volume due to its reduction of speed

be expressed as kinetic energy:

$$E = \frac{1}{2}mv_0^2 \quad (2.1)$$

Subsequently the power can be calculated as the time derivative of the energy:

$$P = \dot{E} = \frac{1}{2}\dot{m}v_0^2 \quad (2.2)$$

The time derivative of the mass can be expressed from the air density ρ , the cross-sectional area A_d and the wind velocity v_0 :

$$\dot{m} = \rho A_d v_0 \quad (2.3)$$

Combining [Eq. \(2.3\)](#) and [Eq. \(2.3\)](#) yields:

$$P_{air} = \frac{1}{2}\rho A_d v_0^3 \quad (2.4)$$

A power coefficient C_p is used to represent the percentage of the available power that is extracted from the wind:

$$P_T = \frac{1}{2}\rho A_d v_0^3 C_p \quad (2.5)$$

C_p is dependent on the rotor blade pitch θ and the tip speed ratio λ . In some of the operating range of a WT the goal is to reach an optimal C_p by adjusting θ and λ to their optimal values:

$$C_p^* = C_p(\theta^*, \lambda^*) \quad (2.6)$$

The achievable size of C_p^* is a matter of the WT design. The *Betz limit* is the highest, optimal C_p that can be theoretically achieved and can be calculated to be:

$$C_{pbetz} = 0.5962 \quad (2.7)$$

Thus efficiency is calculated from the Betz limit:

$$\eta = \frac{C_p}{C_{pbetz}} \quad (2.8)$$

When the air travels over the WT blade the air travels slower on one side than the other as illustrated in [Figure 2](#). Due to mass conservation the air which moves slower on the underside of the blade expands, creating a higher pressure. Likewise the air moving faster on the upper upper side contracts creating in a lower pressure. Resultingly the blade moves upwards.

Blade element momentum theory is often used to model the forces acting along WT blades. Blade element theory involves breaking a blade into small sections and determining the forces acting on that section. In [Figure 3b](#) a cross section

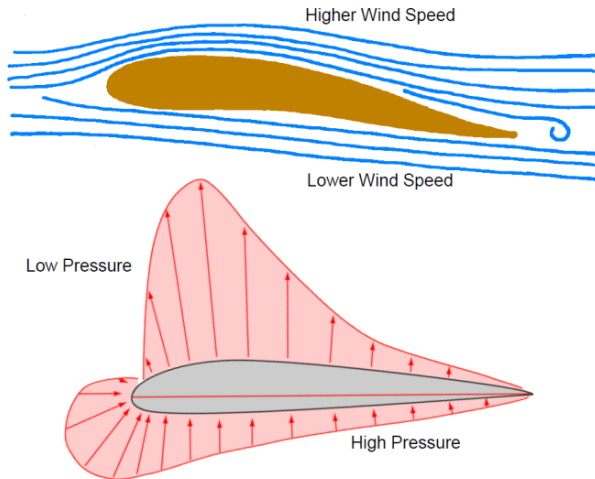
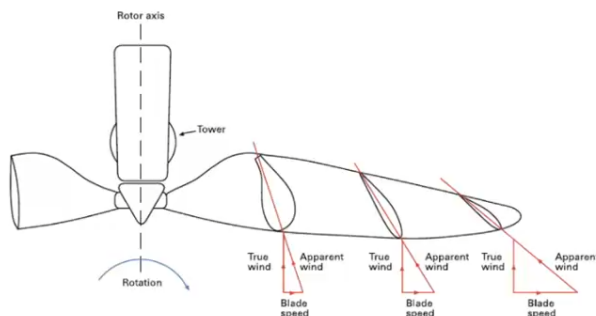
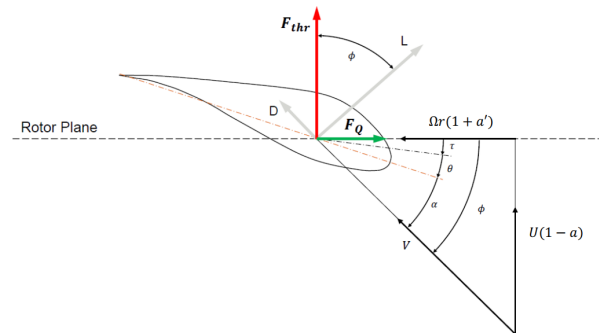


Figure 2: Illustration of the wind speed difference between the two sides of a WT blade along with an illustration of the induced pressure difference. The result is a lifting force on the blade.

of a WT blade can be seen. In this figure, as it is also illustrated at the rotor blade in [Figure 1](#), the wind velocity that hits the rotor blades is lowered indicated by the *axial induction factor* a . What is not observed in [Figure 1](#) is that some of the energy of the wind also goes into driving an airstream around the back of the rotors in the opposite direction of the blade rotation, indicated by the *tangential induction factor* a' .



(a) Velocity triangles along the blade length



(b) Velocity triangle with the rotation induction factor a' included **TO DO: Ensret notation ift. om vindhastighed er U eller v!**

Figure 3: Illustrations of the velocity triangle acting on a cross section of a WT blade

The resulting air speed is V with an *inflow angle* ϕ . L and D is the lift and drag forces respectively. They are calculated from [Eq. \(2.9\)](#) and [Eq. \(2.10\)](#). They include the *chord length* c which is the length from the leading to the trailing edge of the blade and ϕ .

$$L = \frac{1}{2} \rho V^2 c C_L \quad (2.9)$$

$$D = \frac{1}{2} \rho V^2 c C_D \quad (2.10)$$

3 SYSTEM DESCRIPTION

4 MODELLING

4.1 Aerodynamics

5 CONTROLLER DESIGN

6 CONCLUSION

The underlying physics of a trailer refrigeration system are complex, as several components of the system require extensive modeling to accurately represent reality. xxx

7 FUTURE WORK

REFERENCES

- [1] Bp. bp Statistical Review of World Energy. 2022.
- [2] E. Sesto and N. H. Lipman. Wind energy in Europe. 1992.
- [3] Soren Christiansen. Model-Based Control of a Ballast-Stabilized Floating Wind Turbine Exposed to Wind and Waves. 2013.
- [4] Simon Lefebvre and Maurizio Collu. Preliminary design of a floating support structure for a 5 MW offshore wind turbine. *Ocean Engineering*, 40(February 2012):15–26, 2012.

8 APPENDIX

8.1 Link to GitHub Repository

https://github.com/kasperlaustsen/CA8_Project.git

8.2 Explanation of relevant terms for thermodynamics

8.2.1 Enthalpy

Enthalpy is an energy term that is defined as the sum of the flow work.. xx

$$h = u + pv \quad (8.1)$$

8.2.2 Internal energy

The internal energy of a mass can be viewed as primarily.. xx

8.3 List of table lookup symbols

8.4 Linearity of cargo heat transfer coefficient

In order to represent the uncertainty of the cargo coefficient and thus enabling the check for robustness, it is required to show that the linearised system model is linear in UA_{cargo} .. xx

9 DOCUMENTATION AND TESTS

9.1 Test Journal: Evaporator component model

Executed by: xxx

Date: xx/xx/2022

9.1.1 *Objective*

This test aims to document the behavior of the evaporator model with two distinct changes xx..

9.1.2 *Background*

9.1.3 *Test subject*

9.1.4 *Equipment used*

The outputs from a simulation of "eTRU_prototype_2_old_perhaps_with_measurements.slx" are used as inputs for the test xxx..

9.1.5 *Test setup*

9.1.6 *Test procedure*

9.1.7 *Results and Comments*

9.1.8 *Sources of error and insecurities*